



# Development of a model for friction stir weld quality assessment using machine vision and acoustic emission techniques



R. Rajashekar\*, B.M. Rajaprakash

Department of Mechanical Engineering, University Visvesvaraya College of Engineering, Bangalore University, K.R. Circle, Bangalore-560001, Karnataka, India

## ARTICLE INFO

### Article history:

Received 24 April 2015

Received in revised form

15 September 2015

Accepted 16 September 2015

### Keywords:

Friction stir weld

Machine vision

Acoustic emission

Weld strength

Statistical image parameters

X-ray radiography

## ABSTRACT

The surface texture of friction stir weld is related to internal structure of weld. The statistical image parameters along good and defect weld regions are quantitatively evaluated for quality from the weld bead images, which are processed and analyzed using machine vision technique and X-ray radiography. The weld strength obtained along the weld regions showing similar variations in Acoustic Emission (AE) data, which was acquired during welding and image data of the weld bead are analyzed to assess the weld quality. The combined model developed using limiting values of image data and AE data along different regions of weld evaluate the weld quality more reliably.

© 2015 Elsevier B.V. All rights reserved.

## 1. Introduction

The Welding Institute, UK developed Friction Stir Welding (FSW) process in 1991, which is a solid-state, environment friendly joining process which provides improved way of satisfactorily joining aluminum alloys (Thomas et al., 1991). Kumar and Kailas, (2008) investigated the role of FSW tool on material flow and weld formation and reported that the defect free welds are formed by proper shoulder contact with the base material. Suresha et al. (2011) have studied the effect of geometry of tool pin profiles on strength of the welded joints produced using friction stir welding process. It has been reported that the conical pin with threads performed better. Sinha et al. (2008) established linear correlation between the amount of shoulder driven material and the ultimate tensile strength, which controlled the occurrence of defect in friction stir welds by image processing technique. Dwight et al. (2006) examined friction stir welds of aluminum alloys produced using tools with various shoulder geometry and reported that surface roughness and metal deformation in the uppermost layers of welds are greatly influenced by shoulder design. Shaowen and Deng, (2008) carried out combined experimental and numerical investigation of

texture patterns in friction stir welds along different cross sections and found that the banded texture of weld has close ties to the microstructure of the weld region and the bands have a strong effect on the mechanical behavior of welded joints. Scialpi et al. (2007) studied the influence of shoulder geometry on microstructure and mechanical properties of friction stir welds and reported that the interaction of tool shoulder with base material results in different heat input power, which influence the nugget grain dimensions, grain growth and in turn weld strength. From the literatures reviewed by Mishra and Mahoney (2007) on FSW and processing the shoulder surfaces (flat, concave and convex) having features like scroll, ridge or knurling, radial grooves and concentric circles are found to increase the heat generation, deforming more amount of material resulting in increased workpiece mixing and formation of high quality welds.

The outcome of the research on achieving defect free welds show that the weld bead surface, which is formed by the interaction of tool with base material reflects the influence of tool geometry in the formation of weld. Thus, in the present work the banded weld bead surface has been viewed as a characteristic feature for assessment of friction stir weld quality by machine vision technique.

Haralick et al. (1973) suggested twenty eight image textural features which can be extracted from graytone spatial dependence matrix. Venkatramana and Ramamoorthy (1996) and Gadelmawla (2004) quantitatively evaluated image texture of machined surfaces by machine vision and digital image processing techniques

\* Corresponding author.

E-mail addresses: [rajashekar.uvce@gmail.com](mailto:rajashekar.uvce@gmail.com) (R. Rajashekar), [bmruvce@yahoo.co.in](mailto:bmruvce@yahoo.co.in) (B.M. Rajaprakash).

by computing the image properties such as fineness, smoothness, coarseness, granulation, etc., using statistical methods. Bradley and Wong (2001) have described the techniques of use of magnified images of the surfaces generated to assess the condition of the cutting tool in metal cutting. Muthukumar et al. (2008) proposed a methodology for online condition monitoring of the FSW process using image processing technique. The defects and the variations in the quality of weld are indentified by studying the texture pattern of weld bead image from histogram plot, variation in gray level from “line profile plot” and uniformity of weld bead contours from “contour plot”. The line profile plot has the limitation in the sense it considers only the variation in gray values of pixels lying on the line defined. Hence in the present investigation gray values of pixels in a defined region instead of line has been considered using machine vision technique for weld quality assessment.

Acoustic Emission (AE) testing is a powerful Non Destructive Testing (NDT) method of examining the behavior of materials deforming under stress. AE refers to the generation of transient elastic waves produced by a sudden redistribution of stress in a material. When a structure is subjected to an external stimulus (change in pressure, load, or temperature), localized sources trigger the release of energy in the form of stress waves, which propagate to the surface and can be recorded by sensors (Pollock, 2007). Suresha et al. (2009) examined the application of AE technique to analyze the FSW process, which involves deformation, transformation and consolidation of material in solid state under the action of tool. Suresha (2013) studied the behavior of AE data during FSW of similar and dissimilar materials welded using different weld parameters and developed an on-line model to assess the weld quality and to monitor FSW process from the threshold values of AE signals extracted along good and defect weld regions. The contact type AE technique has been employed in this investigation to validate and to improve the reliability of application of machine vision technique.

In this investigation a model for friction stir weld quality assessment has been developed by analyzing the images of weld bead surface produced using optimum weld parameters and tools of different shoulder geometry having Concentric rings and Concave features. The images of weld bead have been processed to quantify the bead texture by evaluating first and second order statistical parameters from histogram and Gray Level Co-occurrence Matrix (GLCM) respectively. The variations in statistical parameters have been studied along good and defect weld regions identified by X-ray radiography results to set threshold values of image parameters. Further, the strength analysis of weld along regions showing variation in AE data, which was acquired during FSW, has been carried out to validate the results of machine vision technique. This improves the reliability of above methodology of machine vision technique, which was limited to occurrence of surface defects. The threshold values of AE data along good and defect weld regions have been combined with that of image parameters for the development of a model, which assess the quality of FSW using both machine vision and AE techniques.

## 2. Experimental details

### 2.1. Friction stir welding

The AA6082-T4 plates of dimensions 300 mm × 75 mm × 5 mm was used with tools of concentric rings and concave shoulder geometry with frustum shaped threaded pin made up of tool steel and the optimum welding parameters for AA6082-T4 employed by Suresha (2013) was adopted: welding speed 100 mm/min, tool rotation speed 1000 rpm, plunge depth 4.85 mm and tool tilt angle 2° for preparing butt welded joints. Table 1 lists the dimensions of the

tools. Two specimens were welded per tool. The first specimen for each tool CN1 (Weld Number 1 produced having concentric rings tool shoulder) and CV1 (Weld Number 1 produced having concave tool shoulder) was welded with plates without holes across thickness to get defect free welds, while second specimen for each tool (CN2 and CV2) was welded with plates having the holes along the thickness to a length of about 10 mm from the butting edge. Welding of plates having holes has been done with an intention to induce defects and study the variations in weld bead texture formed during material consolidation in the defect region by different shoulder geometry.

### 2.2. AE data acquisition

The standard PCI-2 based AE testing equipment of MISTRAS, Physical Acoustics Corporation, U.S.A was used to acquire AE signals during FSW of specimens and the signals were processed and analyzed using AEwin software (Suresha, 2013). The Fig. 1 shows most widely used AE signal parameters namely, Amplitude, RMS, Counts and Energy.

Amplitude (A) is the highest peak voltage attained by an AE waveform. Root Mean Square (RMS) is the rectified, time averaged AE signal (voltage) measured continuously on a linear scale into the AE system. Counts (N) are the threshold-crossing pulses. Energy (E) is the measured area under the rectified signal envelope.

### 2.3. Image data acquisition

The weld bead images were captured off-line using high-resolution digital camera with uniform lighting and processed using Image Processing Tool Box of MATLAB. The Region of Interest (ROI) was defined along good and defect weld regions by comparing with X-ray radiography results. The textures of weld bead images were quantified by extracting statistical image parameters along each ROI. The “First order” statistics involved computation and extraction of significant features such as standard deviation and entropy from the histogram of the images. The “Second order” statistics involved computation and extraction of significant features such as contrast and energy from the GLCM.

Standard deviation measures the average contrast that is sensitive for both smooth and coarse surfaces. Entropy measures randomness of the surface texture. The value of entropy will be higher for coarse texture compared to periodic and smooth texture. This will be most significant parameter to assess banded weld bead texture. Contrast measures the intensity difference between a pixel and its neighbor over the entire image describing smoothness of the image. For the smooth texture, contrast value is 0. energy, which is also known as angular second-moment, measures uniformity of the texture. It considers the sum of square element in the GLCM. For the smooth texture, energy value is 1.

The tensile specimens were extracted along the regions of defect free welds, which revealed variations in AE data to study the variations in the strength of weld. The base material AA6082-T4 is a medium strength aluminum alloy with excellent corrosion resistance and Table 2 lists its mechanical properties. The tensile specimens were prepared as per ASTM-E8/EM-08 standards shown in Fig. 2 along the direction perpendicular to tool traverse and tested on Electronic Tensometer.

## 3. Results and discussion

The effectiveness of the shoulder in forming defect free weld was evaluated by the amount of surface roughness, and uniformity of weld bead produced during welding (Burford et al., 2006) using workpiece with and without holes across the thickness in the butting edge. The statistical image parameters obtained for different

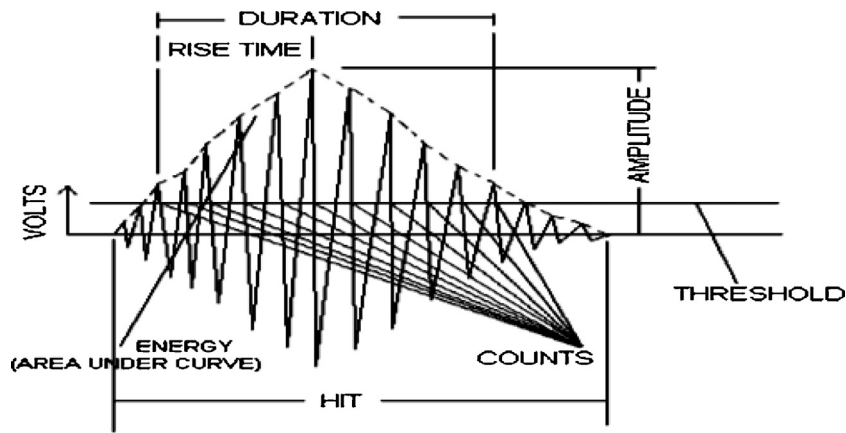


Fig. 1. Commonly measured parameters of a burst type AE signals (Suresha, 2013).

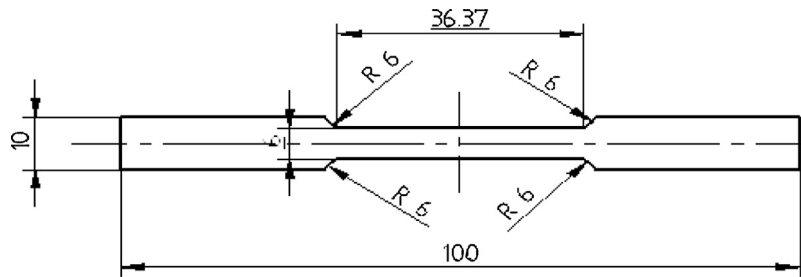


Fig. 2. Dimensions of tensile test specimen.

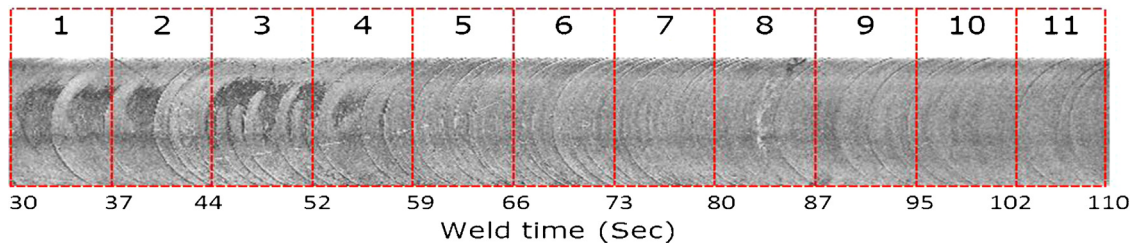


Fig. 3. Processed weld bead image of CN1 and equal size of ROI defined to extract the image data.

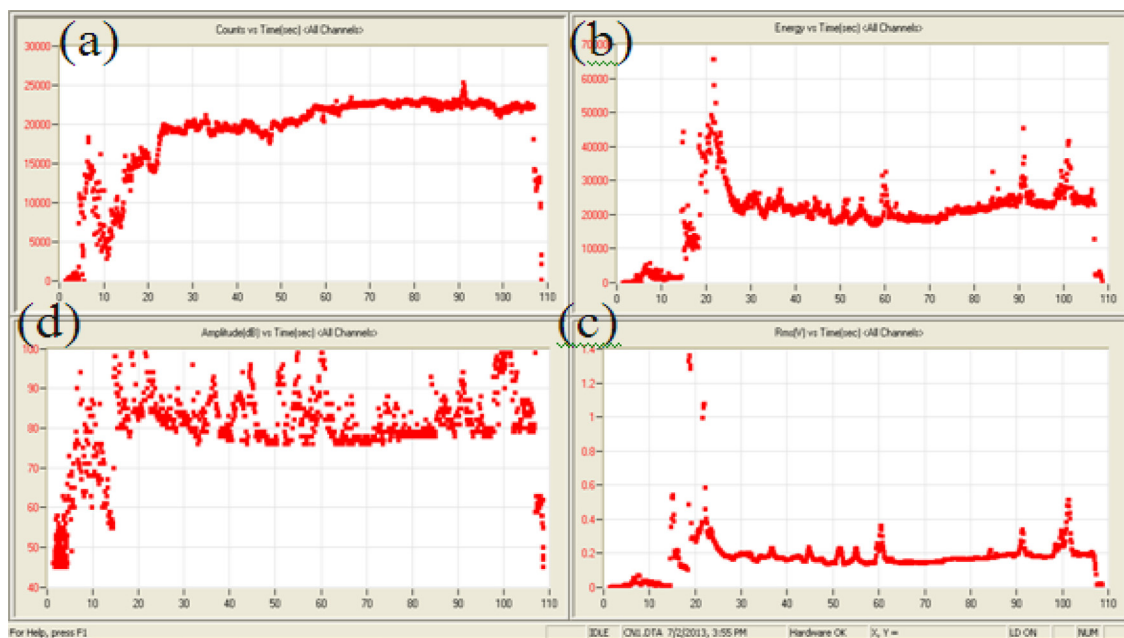




Fig. 4. AE signal data: (a) Counts, (b) Energy, (c) RMS and (d) Amplitude acquired during FSW of CN1.

**Table 1**  
FSW Tool dimensions and shoulder geometries.

Tool Dimensions (mm)	Tool type	
	Concentric circle shoulder with conical threaded pin (CN)	Concave shoulder with conical threaded pin (CV)
Pin length	4.7	
Pin diameter	Larger = 6 Smaller = 4	
Shoulder diameter	20	
Shoulder length	25	
LH thread pitch	1	





Concavity = 6°–7°

**Table 2**  
Mechanical Properties of base material AA6082-T4.

Yield Strength (N/mm <sup>2</sup> )	Ultimate Tensile Strength (N/mm <sup>2</sup> )	Shear Strength (N/mm <sup>2</sup> )	Hardness Vickers (HV)
291	305	210	100

**Table 3**  
Regions of Tensile specimens' extractions and AE data of CN1.

Tensile specimens	ROI	Weld region (sec)	AE data RMSchar.dot (V)	Energy × 10 <sup>3</sup>	Counts × 10 <sup>3</sup>	Amplitude (dB)
T1	3	45–52	0.21–0.18	25–18	20–16	90–76
T2	7	75–85	0.2–0.17	21–19	24–23	88–78
T3	9	90–100	0.38–0.18	30–21	25–22	94–78
T4	11	105–110	0.5–0.18	36–21	23–21	100–79

**Table 4**  
Strength of tensile specimens of CN1.

FSW specimens	Tensile specimens	Ultimate Tensile Strength (N/mm <sup>2</sup> )		Joint efficiency (%)	Standard deviation
		Engg.	Average		
CN1	T1	198.1	198.5	64.53	0.5
	T2	198.1			
	T3	198.8			
	T4	199.1			

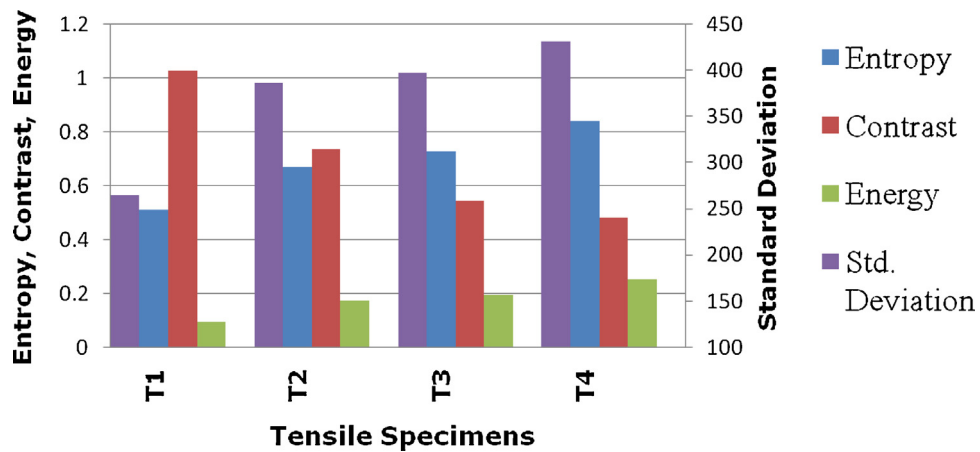


Fig. 5. Plot of statistical image parameters along ROI of different tensile strength of CN1.

**Table 5**  
Statistical image parameters along tensile specimens of CN1.

Tensile specimens	Weld regions (ROI)	First order		Second order	
		StandardDeviation	Entropy	Contrast	Energy
T1	3	321.77	0.6620	0.8201	0.128
T2	7	386.51	0.6708	0.7344	0.175
T3	9	397.73	0.7281	0.5432	0.195
T4	11	431.99	0.8408	0.4830	0.254

**Table 6**  
Statistical image parameters of CN2.

Weld regions(ROI)	First order		Second order	
	Standard deviation	Entropy	Contrast	Energy
1	236.54	0.3060	0.8053	0.1020
3	251.81	0.4093	0.9024	0.1084
5	193.27	0.2897	1.3327	0.0713
7	228.13	0.1809	1.2866	0.0890
9	197.95	0.1603	1.3502	0.0717
12	254.67	0.3671	0.8043	0.1125

ROI showed variation in their values, which enabled to establish the criteria for weld quality assessment.

Fig. 3 shows the processed weld bead image of CN1 welded with plates without holes across cross section using concentric rings shoulder geometry tool and equal size of ROI defined to extract the image data, X-ray radiography of CN1 showed no defect in the weld. Fig. 4 shows the variations in AE signal data acquired during FSW of CN1. Table 3 lists the ROI (3, 7, 9 and 11), tensile specimens and AE data extracted along corresponding ROI. The weld bead texture of ROI (3, 7, 9 and 11) was quantified by extracting first order and second order statistical image parameters. The tensile strength of specimens as listed in Table 4 was correlated with image parameters plotted in Fig. 5 and which is has been listed in Table 5 to assess the defect free weld.

Fig. 6 shows processed weld bead image of CN2 welded by butting the edges of the plates with holes across cross section using concentric rings shoulder geometry tool and equal size of ROI defined to extract the image data, X-ray radiography of CN2 as shown in Fig. 7 shows defects in the weld. Fig. 8 shows variation of AE signal data acquired along defective regions of weld CN2.

The weld bead texture along ROIs 1, 3, 5, 7, 9 and 12 are considered for analysis was quantified and variations in first and second order statistical image parameters are as listed in Table 6 and plotted in Fig. 9.

Based on the above experiments conducted using concentric rings shoulder tool, it can be concluded that, among the tensile specimens of CN1, T4 which showed high strength (Table 4) was extracted from the region showing large variation in AE data (RMS, energy and amplitude) with less count. This may be attributed to presence of concentric rings features beneath the shoulder resulting in more frictional heat, which increased the surface deformation facilitating better consolidation of material at the interface. The weld bead texture of this region was characterized by higher entropy and energy value relative to other regions considered for strength analysis due to the increased uniformity of the weld bead surface. The Tensile specimens T1 and T2 showed low strength (Table 4), though they experiences relatively low variations in AE data (RMS, energy and amplitude) when compared to that of T4. This may be attributed to insufficient frictional heat resulted by reduced surface interaction during welding. This was indicated by image data, which characterized weld bead surface as rough showing higher value of contrast and non-uniform showing lower value of energy.

The CN2 showed defect regions around the holes which extended along weld line due to lack of fusion as seen from the X-ray radiography results of CN2 (Fig. 7). The weld bead was

**Table 7**  
Threshold values of AE data of CN2.

Weld regions	RMS (V)	Energy $\times 10^3$	Counts $\times 10^3$	Amplitude (dB)
Good	0.5–0.17	36–18	24–21	100–76
Defect	0.17	0–18	2–16	76–58

characterized by increased contrast, standard deviation, reduced entropy and energy. This resulted in rough, alternate dark and bright-banded texture due to the presence of concentric rings. The threshold values of statistical image parameters and AE data (Table 7) were arrived from the analysis of ROI of CN1 and CN2 along good and defect weld regions for the development of model for weld quality assessment using both machine vision technique and AE technique for concentric rings shoulder geometry tool which is as shown in Fig. 10.

Fig. 11 shows processed weld bead image of CV1 welded with plates without holes across cross section using concave shoulder geometry tool and equal size of ROIs defined along weld. The X-ray radiography of CV1 showed no defect in the weld. Fig. 12 shows the variations in AE signal data acquired during FSW of CV1. Table 8 lists the different ROIs, tensile specimens and AE data extracted along corresponding ROI. The strength of specimens as listed in Table 9 is correlated with image parameters, which is as listed in Table 10 and plotted as shown in Fig. 13 and to assess the defect free weld.

Fig. 14 shows the processed weld bead image of CV2 welded by butting the edges of the plates with holes across cross section using concave shoulder geometry tool and equal sizes of ROI defined along weld region. The X-ray radiography of CV2 as shown in Fig. 15 shows no defects in the weld. The variation of AE signal data along regions of defect free weld of CV2 is as shown in Fig. 16. Table 11 lists the first and second order statistical image parameters which were quantified by processing ROIs along defect free weld regions and the plot of which is as shown in Fig. 17. The variation in statistical image parameters in conjunction with AE signal data were studied to understand the variations in bead texture along hole and no hole regions during FSW of CV2. The welded joints (CV1 and CV2) prepared by concave shoulder tool resulted in producing defect free welds. Therefore limiting values of image and AE data along defect weld regions is arrived by assuming probable occurrence of defects at lesser values of image and AE data recorded at hole regions.

Based on the above experiments conducted using concave shoulder tool, it can be concluded that, the tensile specimen T1 of CV1 which showed high strength (Table 9) was extracted along the weld region which showed low variation in AE data in the upper range. This was due to initial stage of tool traverse along the material of high heat content during welding. The weld bead of this region was characterized by reduced roughness with uniform texture as indicated by higher values of entropy and energy and the reduced values of Contrast compared to that of other ROI's which were considered for strength analysis.

The tensile specimen T4 which showed low strength (Table 9) was extracted along the region which showed large variation in RMS, energy and amplitude with small variation in counts at higher value. This may be attributed to accumulation of heat at the end closure to the end of the weld. Energy, which is expressed as MARSE is the measure of area under the rectified signal envelope and it is sensitive to amplitude as well as duration and indicates

**Table 8**  
Regions of Tensile specimens' extractions and AE data of CV1.

Tensile specimens	ROI	Weld region (sec)	RMS (V)	Energy $\times 10^3$	Counts $\times 10^3$	Amplitude (dB)
T1	2	45–55	0.3–0.25	36–30	22–21	83–78
T2	3	55–60	0.35–0.21	40–30	22–21	85–80
T3	10	110–115	0.25–0.2	31–28	23–21	88–80
T4	13	130–138	0.38–0.2	37–28	24–22	96–80

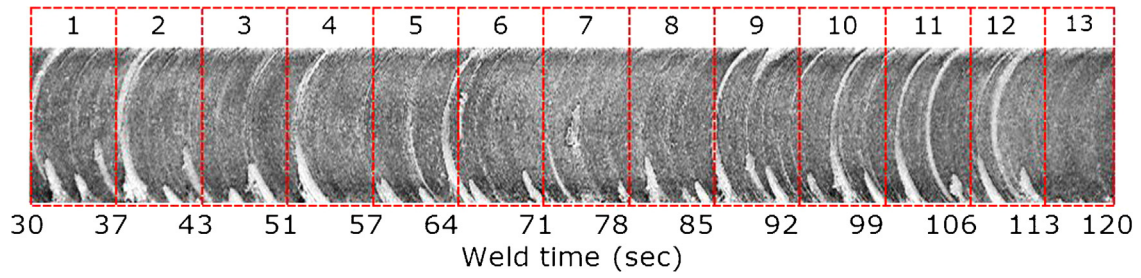


Fig. 6. Processed weld bead image of CN2 and equal size of ROI defined to extract the image data.

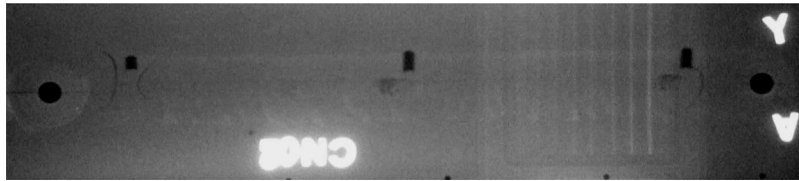


Fig. 7. X-ray radiography of CN2 showing defects.

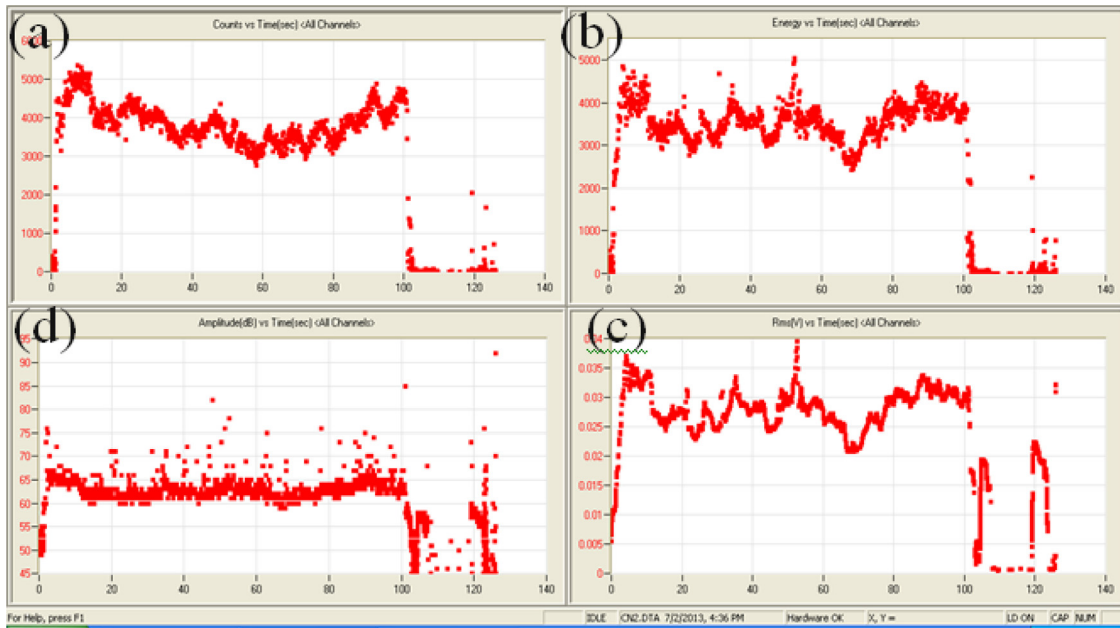


Fig. 8. AE signal data: (a) Counts, (b) Energy, (c) RMS and (d) Amplitude acquired during FSW of CN2.

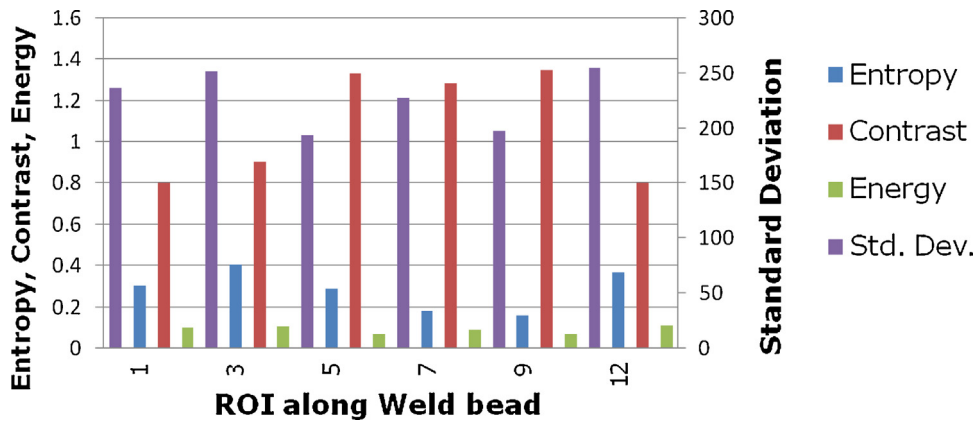


Fig. 9. Plot of statistical image parameters of CN2.

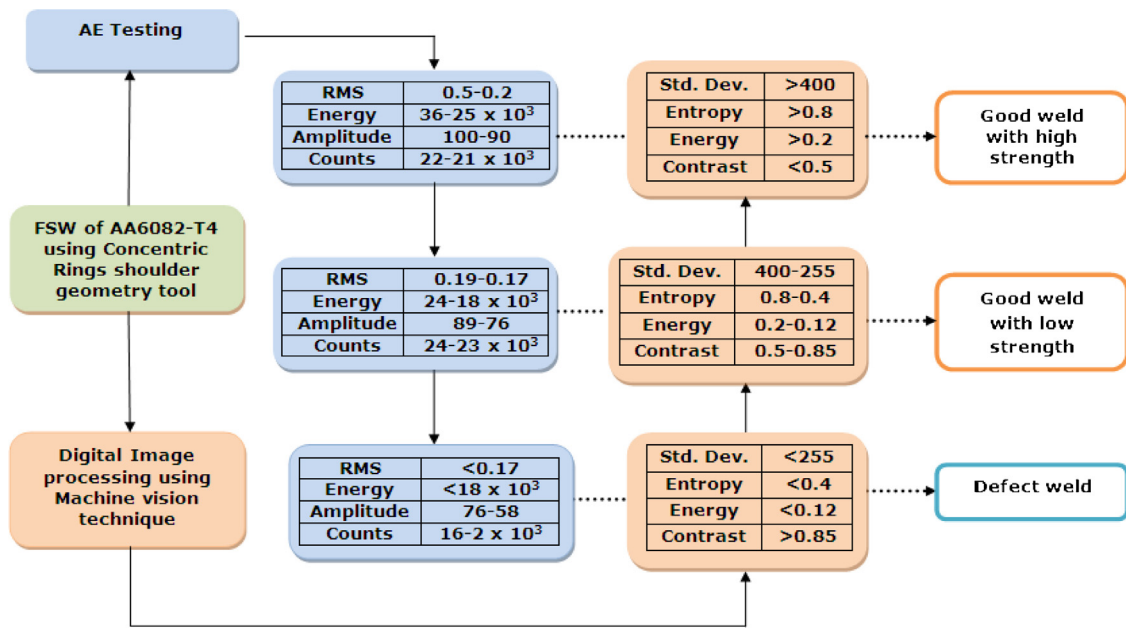


Fig. 10. Friction stir weld quality assessment model for concentric rings shoulder geometry tool.

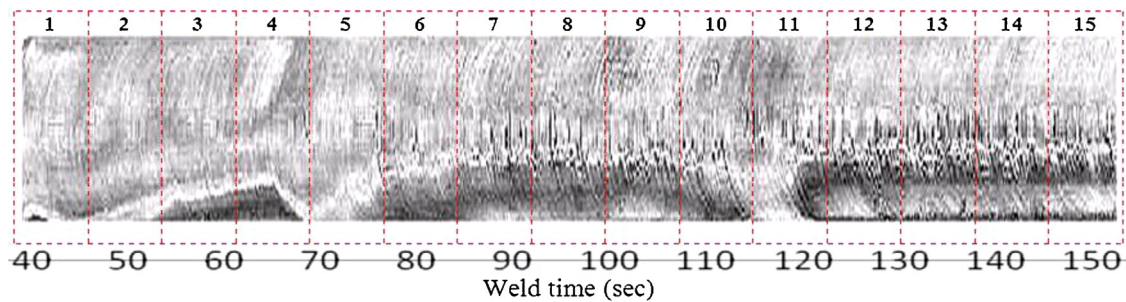


Fig. 11. Processed weld bead image of CV1, weld time and equal size of ROI defined to extract the image data.

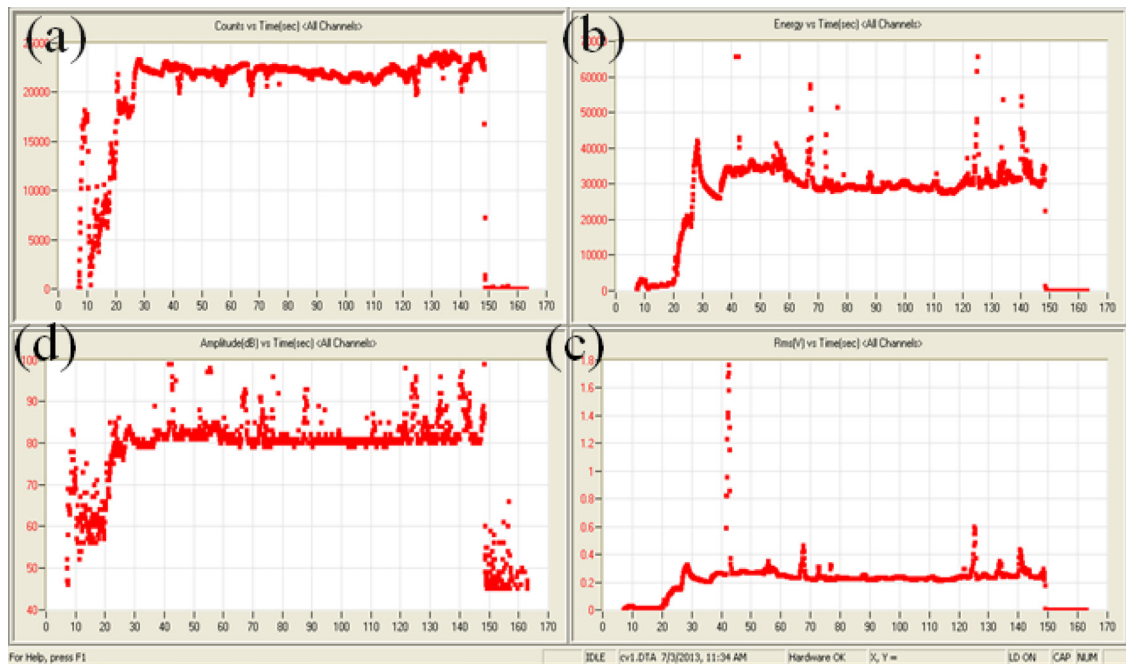


Fig. 12. AE signal data: (a) Counts, (b) Energy, (c) RMS and (d) Amplitude acquired during FSW of CV1.

**Table 9**  
Strength of tensile specimens of CV1.

FSW specimens	Tensile specimens	Ultimate tensile strength (N/mm <sup>2</sup> )		Joint efficiency (%)	Standard deviation
		Engg.	Average		
CV1	T1	201.7	199.3	64.79	3.26
	T2	200.7			
	T3	200.4			
	T4	194.5			

**Table 10**  
Statistical image parameters along tensile specimens of CV1.

Tensile specimens	Weld regions (ROI)	First order		Second order	
		Standard deviation	Entropy	Contrast	Energy
T1	2	367.73	0.9947	0.4455	0.2527
T2	3	336.16	0.9209	0.4727	0.2143
T3	10	329.57	0.8774	0.5409	0.2201
T4	13	267.36	0.5960	0.6001	0.1620

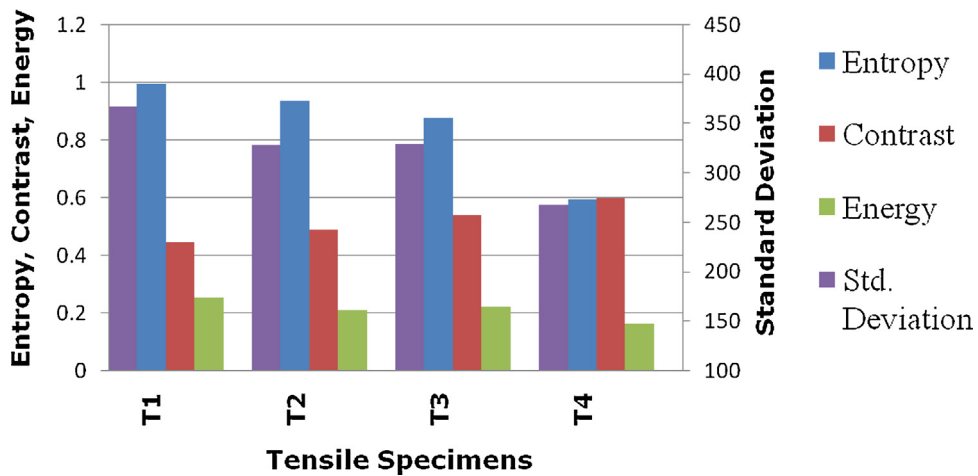


Fig. 13. Plot of statistical image parameters along ROI of different tensile strength of CV1.

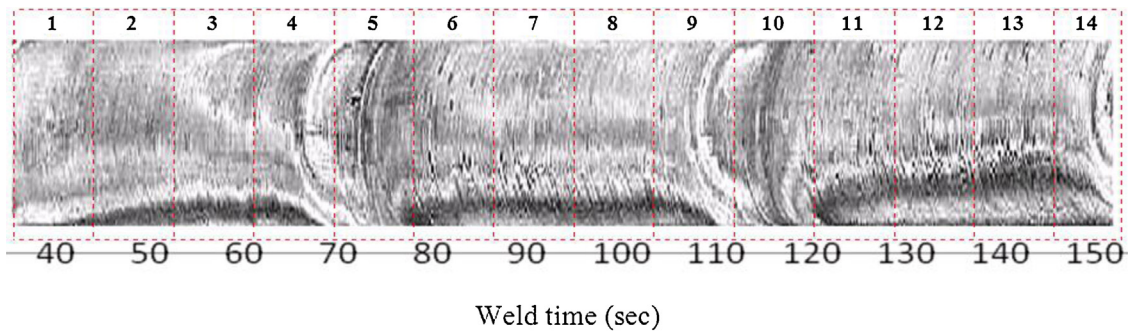


Fig. 14. Processed weld bead image of CV2, weld time and equal size of ROI defined to extract the image data.

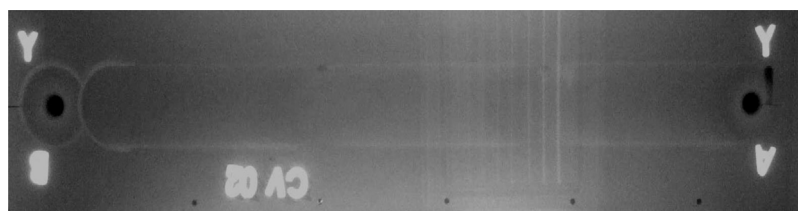


Fig. 15. X-ray radiography of CV2 showing no defects.



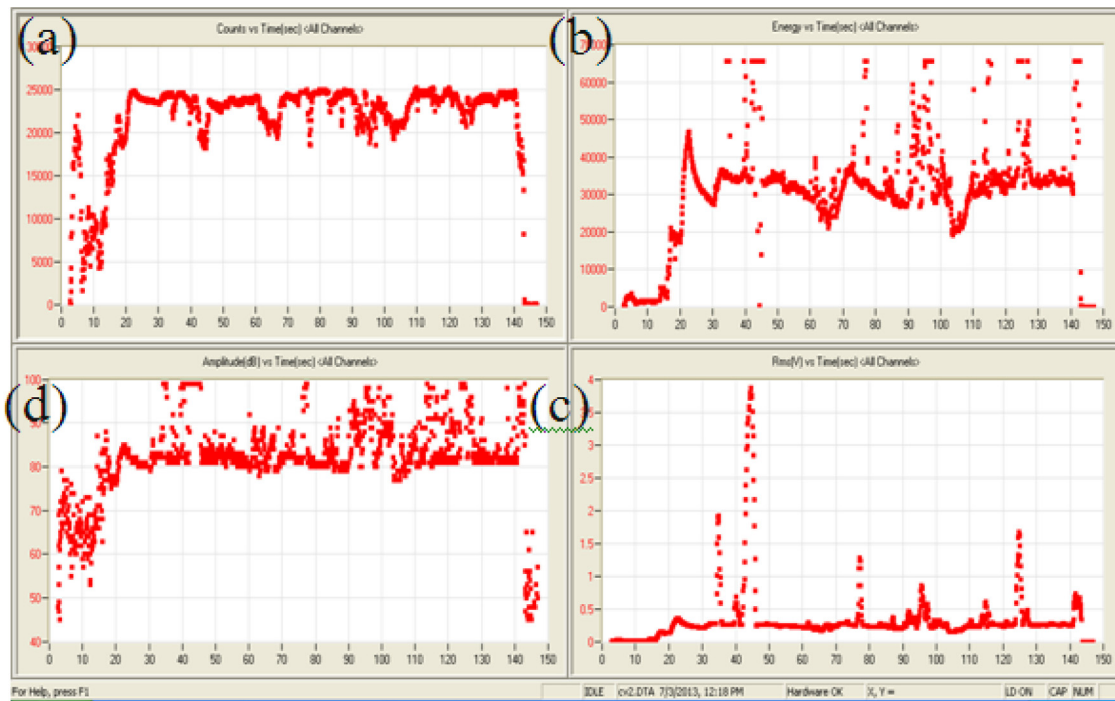


Fig. 16. AE signal data: (a) Counts, (b) Energy, (c) RMS and (d) Amplitude acquired during FSW of CV2.

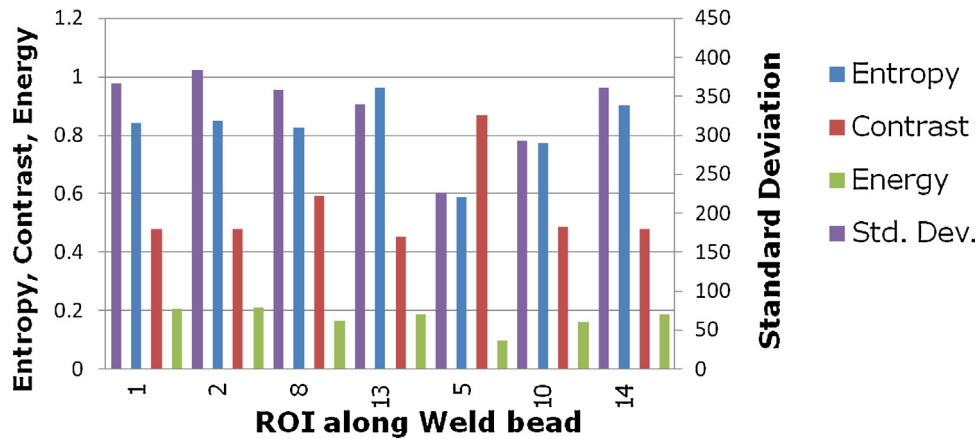


Fig. 17. Plot of statistical image parameters (ROI 5 and 10 along hole region) of CV2.

more AE activities within the small duration of weld length of T4 generating more frictional heat which resulted in increased temperature. The weld bead of this region was characterized by rough and non-uniform texture. The tensile specimen T2 has less strength compared to T1, it was extracted in the region where the transition of AE values from higher value to lower value have occurred which resulted in large variation of AE data compared to that of T1 region with same value of counts. This may be due the heat conducting through the material ahead and thus stabilizing the temperature. The reduced strength was indicated by the bead texture of less uniformity.

The texture along the hole regions (ROI 5, 10) of CV2 showed highly deformed coarse, uneven and distorted texture. The statistical image parameters along these regions show reduced value of standard deviation, entropy and energy and increased value of contrast along ROI 5. This may be due to the highly deformed material interface observed around the hole region due to increased temperature, which resulted from reduced heat transfer as there is no material (hole) in front of the tool. Along the 2nd hole region (ROI

Table 11  
Statistical image parameters of CV2.

Weld regions(ROI)	First order		Second order	
	Standard Deviation	Entropy	Contrast	Energy
1	366.59	0.8408	0.4759	0.2061
2	383.12	0.8464	0.4785	0.2068
5(Hole region)	225.38	0.5859	0.8685	0.0957
8	357.23	0.8234	0.5896	0.1611
10(Hole region)	291.89	0.7720	0.4832	0.1575
13	339.02	0.9626	0.4521	0.1838
14	360.00	0.9004	0.4775	0.1853

10) the improvement in texture compared to that of ROI 5 was observed due proper consolidation of material with reduced temperature as the tool traversed large distance from 1st hole region stabilizing the weld temperature. The statistical image parameters showed increased values of entropy and decreased values contrast (roughness) and energy. The standard deviation shows higher value

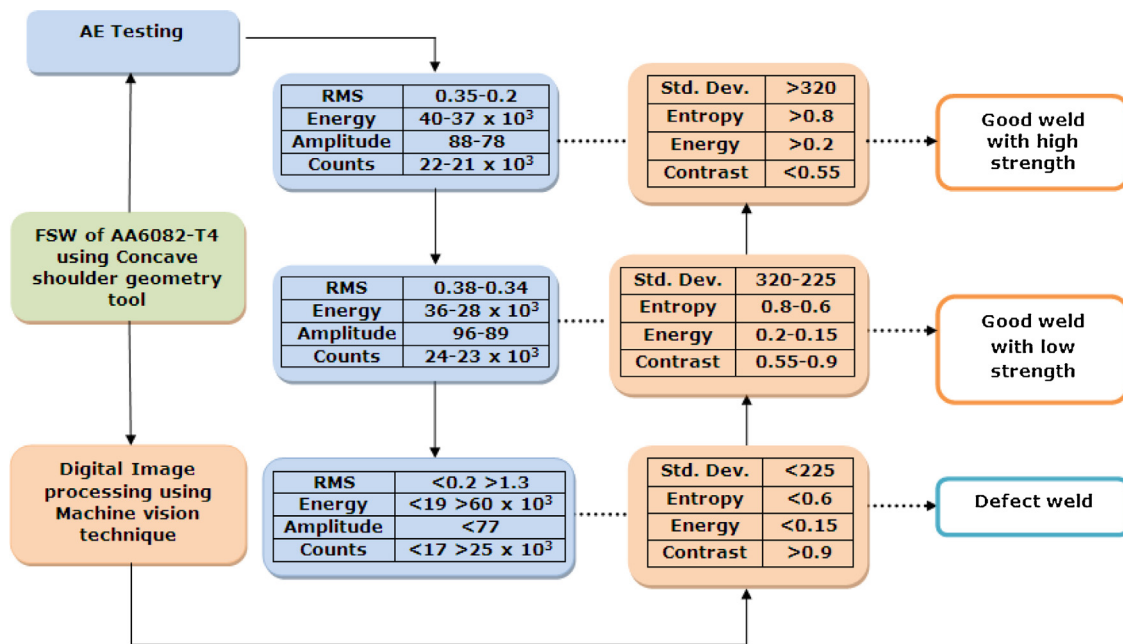


Fig. 18. Friction stir weld quality assessment model for concave shoulder geometry tool.

Table 12  
Threshold values of AE data of CV2.

Weld regions	RMS (V)	Energy × 10 <sup>3</sup>	Counts × 10 <sup>3</sup>	Amplitude (dB)
Good	0.38–0.2	40–28	24–21	96–78
Defect	<0.25 >1.3	<19 >60	<17 >25	<77

as it was sensitive to variation in contrast. The threshold values of statistical image parameters and AE data (Table 12) arrived from analysis of ROI's of CV1 and CV2 along good weld regions were considered for the development of model for weld quality assessment using both machine vision technique and AE technique for concave shoulder geometry tool as shown in Fig. 18.

#### 4. Conclusions

The following conclusions have been drawn from the results and discussion:

- The weld bead texture of welds obtained using tool with concentric rings shoulder was characterized by distorted and non-uniform distribution of image texture elements due to the presence of concentric rings.
- The weld bead texture of welds produced using concave tool shoulder geometry was characterized with evenness and uniformity in the distribution of image texture elements, which reduced roughness.
- It is evident from the appearance of weld bead surface that due to presence of concave geometry of the shoulder, which showed better interaction and consolidation of material resulting in the formation of defect free welds.
- The variation in statistical image parameters is observed along different regions of weld and depends on the tool shoulder geometry.
- The variations observed for AE data along different regions of weld are similar to that of variations in image parameters.
- The machine vision and AE are successfully integrated for reliable assessment of weld quality.

#### Acknowledgements

Authors would like to thank assistance provided in sharing AE equipments and FSW specimens for AR&DB project funded by Aeronautical Research & Development Board (AR&DB project 1473) and Dr. Satish V. Kailas, Professor, Department of Mechanical Engineering, IISc, Bangalore for extending FSW machine facilities.

#### References

- Bradley, C., Wong, Y.S., 2001. Surface texture indicators of tool wear—a machine vision approach. *Int. J. Adv. Manuf. Technol.* 17, 435–443.
- Burford, Dwight A., Tweedy, Bryan M., Widener, Christian A., 2006. Influence of shoulder configuration and geometric features on FSW track properties. *Proceedings of sixth International Symposium on Friction Stir Welding*.
- Gadelmawla, E.S., 2004. A vision system for surface roughness characterization using the gray level co-occurrence matrix. *NDT & E Int.* 37, 577–588.
- Haralick, Robert M., Shanmugam, K., Dinstein, Itshak, 1973. Textural features for image classification. *IEEE Trans. Syst. Man Cybern.* 6, 610–621.
- Kumar, K., Kailas, Satish V., 2008. The role of friction stir welding tool on material flow and weld formation. *Mater. Sci. Eng. A* 485, 367–374.
- Mishra, Rajiv S., Mahoney, Murray W., 2007. *Friction Stir Welding and Processing*. ASM Int, editors.
- Muthukumar, S., Sinha, Preetish, Sivakumar, R., Mukherjee, S.K., 2008. Condition monitoring of first mode of metal transfer in friction stir welding by image processing techniques. *Int. J. Adv. Manuf. Technol.* 36, 484–489.
- Pollock, Adrian A., 2007. *PCI-2 Based Ae System User's Manual*. Physical Acoustics Corporation, USA.
- Scialpi, A., De Filippis, L.A.C., Cavaliere, P., 2007. Influence of shoulder geometry on microstructure and mechanical properties of friction stir welded 6082 aluminium alloy. *Mater. Des.* 28, 1124–1129.
- Shaowen, X.U., Deng, Xiaomin., 2008. A study of texture patterns in friction stir welds. *Acta Mater.* 56, 1326–1341.
- Sinha, Preetish, Muthukumar, S., Mukherjee, S.K., 2008. Analysis of first mode of metal transfer in friction stir welded plates by image processing technique. *J. Mater. Process. Technol.* 197, 17–21.
- Suresha, C.N., Rajaprakash, B.M., Upadhy, S., 2009. Applicability of acoustic emission in the analysis of friction stir welded joints. *Int. J. Recent Trends Eng.*
- Suresha, C.N., Rajaprakash, B.M., Sarala, U., padhya, 2011. A study of the effect of tool pin profiles on tensile strength of welded joints produced using friction stir welding process. *Mater. Manuf. Processes* 26, 1111–1116.
- Suresha, C.N., 2013. *Studies on performance of welded joints produced by friction stir welding process using acoustic emission technique*. In: Ph.D Thesis. Bangalore University.
- Venkatramana, K., Ramamoorthy, B., 1996. Statistical methods to compare the texture features of machined surfaces. *Pattern Recognit.* 29, 1447–1459.
- Thomas W.M., Nicholas E.D., Needham J.C., Murch M.G., Templesmith P., Daws C.J., 1991. Friction stir butt welding. International Patent Application No PCT/GB92/02203, GB Patent Application 9125978, 8, UK Patent Office, London.